

# Precision open-loop control of piezoelectric actuator

Zhigang Nie<sup>1</sup>, Yuguo Cui<sup>1</sup> , Jun Huang<sup>1</sup>, Yiqiang Wang<sup>2</sup> and Tehuan Chen<sup>1</sup>

## Abstract

Due to space constraints, some micro-assemblies and micro-operating systems cannot install sensors, so it is challenging to achieve closed-loop control. For this reason, a precision open-loop control strategy for piezoelectric actuators is proposed. Firstly, based on the PI model and the proposed threshold partition method, the hysteresis model of the piezoelectric actuator with rate-dependent and few operators is established. Then the hysteresis error of the piezoelectric actuator is compensated by the inverse model obtained. Secondly, the creep model of the logarithmic piezoelectric actuator with simple expression and few parameters is established. Then, a creep controller without demand inverse is designed to compensate for the creep error of the piezoelectric actuator. Finally, a ZVD (Zero Vibration Derivative) input shaping method with good robustness is given to eliminate the oscillation generated by the piezoelectric actuator under the action of the step signal. The experimental results show that the displacement error of piezoelectric actuator is reduced from  $-9.07$  to  $9.46\ \mu\text{m}$  to  $-1.22$  to  $1.78\ \mu\text{m}$  when the maximum displacement is  $120\ \mu\text{m}$  after hysteresis compensation; after creeping compensation, within the action time of the  $1200\ \text{s}$ , the displacement creep of the piezoelectric actuator was reduced from  $5.5\ \mu\text{m}$  before compensation to  $0.3\ \mu\text{m}$ ; after the oscillation control, the displacement overshoot of the piezoelectric actuator is reduced to  $0.6\%$  of that before control.

## Keywords

Piezoelectric actuator, hysteresis modeling and compensation, creep modeling and compensation, dynamics modeling, oscillation suppression

## 1. Introduction

As a high-performance functional device, the piezoelectric actuator has the advantages of small size, high displacement resolution, fast response speed, compact structure, large driving force, and low cost. Therefore, it has a broad application prospect in the fields of micro-assembly (Heriban et al., 2008), intelligent structure (Gao et al., 2020; Tanaka, 2014), precision machining (Lin et al., 2016), nanotechnology (Gu et al., 2016; Li et al., 2019), bioengineering (Zainal et al., 2015). For example, it is used in the assembly of micro-parts (Schröter and Schmidt, 2018), the probe positioning of scanning probe microscope (Lu et al., 2018), the clamping of cells in bioengineering (Garcés-Schröder et al., 2015; Kim et al., 2008). However, as a ferroelectric material, the piezoelectric actuator has nonlinear characteristics such as hysteresis and creep (Li et al., 2015; Sabarianand et al., 2020), and it is easy to oscillate under the action of step and pulse signals, which will affect the operation accuracy of micro-assembly and micro-operating system driven by a piezoelectric actuator.

In order to improve the operation accuracy of the system driven by piezoelectric actuators, corresponding control methods need to be adopted to eliminate the nonlinear characteristics such as hysteresis, creep, and oscillation of piezoelectric actuators. These control methods include feedforward control, feedback control, and compound control. Feedforward control is based on the model, so it is necessary to establish a mathematical model to describe the hysteresis, creep, and oscillation characteristics of piezoelectric actuators. In the aspect of hysteresis modeling of piezoelectric actuators, Jia et al. used the Preisach model to describe the hysteresis characteristics of piezoelectric actuators and used

<sup>1</sup>School of Mechanical Engineering and Mechanics, Ningbo University, Ningbo, China

<sup>2</sup>School of Mechatronics and Energy Engineering, Ningbo Institute of Technology, Zhejiang University, Ningbo, China

## Corresponding author:

Yuguo Cui, School of Mechanical Engineering and Mechanics, Ningbo University, 888 Fenghua Road, Ningbo 315211, China.

Email: cuiyuguo@nbu.edu.cn

the least square support vector machine method to identify the hysteresis model built (Jiaqiang et al., 2017; Krejčí and Monteiro, 2019); Son et al. used the Bouc-Wen model to describe the hysteresis characteristics of piezoelectric actuators, and proposed a hybrid adaptive difference evolution and Jaya algorithm (aDE-Jaya) to identify the hysteresis model of piezoelectric actuators (Qian et al., 2020; Son et al., 2020); Wang et al. used the Duhem model to establish the hysteresis model of piezoelectric actuators (Lin and Lin, 2012; Wang and Chen, 2017); Lee et al. (2000) studied the hysteresis characteristics of piezoelectric ceramic transducers theoretically and experimentally, and established a rate-independent generalized Maxwell resistance-capacitance (MRC) hysteresis model; Li et al. used the Dahl model to establish the dynamic hysteresis model of the piezoelectric actuator, and use particle swarm optimization to identify it, which improves the hysteresis compensation accuracy of the piezoelectric actuator (Xu and Li, 2010); Qin et al. updated the weight of the Backlash operator according to the input rate to illustrate the rate-related characteristics, and proposed an improved Prandtl-Ishlinskii (PI) hysteresis model (Al Janaideh et al., 2018; Qin et al., 2017). PI model has the advantages of a few parameters, non-cumulative errors, and easy inversion, so it is widely used to describe the hysteresis characteristics of objects. However, there are often some invalid operators with zero weight in this model, which will reduce the response speed of the controlled object. In the aspect of creep modeling of piezoelectric actuators, Liu et al. expressed piezoelectric actuators as resistance and capacitance. They proposed a fractional creep model (Liu et al., 2013), which does not need to find inverse in control, but it is too complex and challenging to identify. Chang et al. use the hysteresis inverse model, including creep characteristics as a feedforward controller to compensate for the creep of piezoelectric actuators, this method has high accuracy, but the model inversion is complex (Changhai and Lining, 2005). The ideal creep model should have a simple expression, few parameters, and no demand inverse. When establishing the mathematical model to describe the oscillation characteristics of piezoelectric actuators, the hysteresis and creep characteristics of piezoelectric actuators are not considered, but only the linear dynamic model is established, and the system identification method is used to identify the linear dynamic model. These identification methods include MATLAB system identification toolbox (Habibullah et al., 2013), weighted iterative least square fitting method (Lee and Salapaka, 2009), state-space system identification method based on subspace (Schitter et al., 2004). In the aspect of vibration control of piezoelectric actuators, it is mainly based on the axiomatic design theory in the time domain (Li et al., 2010), in which the commonly used method is ZV (Zero Vibration) input shaping method, which is simple in principle and easy to implement, but when the system damping is small, the

robustness becomes worse. The feedforward control needs no sensor and has a low cost. The designed hysteresis model controller, creep model controller, vibration model controller, and piezoelectric actuator are connected in series. The precision of the model determines the control precision.

In the aspect of feedback control, Chen et al. (2016) used a minimum parameterized hysteresis model to reduce the amount of calculation and designed an achievable adaptive controller. Liaw et al. proposed a robust impedance control scheme for piezoelectric-driven flexible four-bar micro-nano manipulators (Liaw and Shirinzadeh, 2008). Xu et al. designed a new output-based digital integral terminal sliding mode predictive control (DITSMPC) scheme for precise motion control of the piezoelectric actuator, significantly reducing the hysteresis error piezoelectric actuator (Xu and Member, 2016). Feedback control has good accuracy because sensors in real-time feedback its signals, but the system cost is high. In some micro-assembly and micro-operating systems, due to space constraints, sometimes sensors cannot be installed.

Compound control is the combination of feedforward control and feedback control introduced above. That is, the inverse hysteresis model is connected in series with the piezoelectric actuator, and the feedback signal is presented to design the controller. Tan et al. proposed an adaptive inverse control scheme by updating the Preisach operator (Tan and Baras, 2004); Gan et al. (2017) designed an adaptive inverse control based on an improved Prandtl-Ishlinskii (PI) model and achieved good hysteresis tracking performance; Kim et al. (2012) designed a sliding mode predictive control with the inverse model, which significantly reduced the hysteresis effect. The all-around performance of the compound control is good, but it is also limited by space. Sometimes the sensor can not be installed, and the cost of the system is high.

To reduce the cost of micro-assembly and micro-operating system and to ensure that the system still has high operating accuracy when space is limited, an open-loop controller is designed in this paper to eliminate the hysteresis, creep, and oscillation of the piezoelectric actuator. In order to improve the control accuracy, each behavior is modeled independently. Modeling, identification, and compensation are carried out step by step and then realize its precise open-loop control, specifically: taking the piezoelectric bimorph actuator as the object (as shown in Figure 1, the piezoelectric bimorph cantilever beam bends when it is excited by electricity). Firstly, based on the PI model and the proposed threshold partition method, the hysteresis model of the piezoelectric actuator with rate-dependent and few operators is established, and then the hysteresis error of the piezoelectric actuator is compensated by the inverse model. Secondly, based on eliminating the hysteresis of piezoelectric actuators and based on the

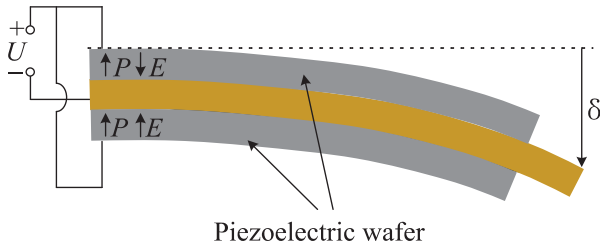


**Figure 1.** Piezoelectric bimorph cantilever beam.

proposed logarithmic piezoelectric creep model, a creep controller without demand inversion is designed to compensate for the creep error. Finally, based on eliminating the hysteresis and creep of the piezoelectric actuator, the ZVD input shaping method is proposed to eliminate the system's oscillation.

This paper is organized as follows: the second section introduces establishing the hysteresis static model and dynamic hysteresis model of the piezoelectric actuator and the simulation of hysteresis compensation for the inverse model. In addition, it also introduces the experimental system for testing the open-loop control of the piezoelectric actuator. The third section introduces the establishment of the creep model and creeps compensation simulation of piezoelectric actuator after hysteresis compensation. The fourth section presents the dynamic modeling and oscillation suppression simulation of the creep and hysteresis compensation system. The fifth section introduces in detail the experimental verification of the proposed compensation method. Finally, the sixth section summarizes this paper.

## 2. Hysteresis compensation

The PI hysteresis model is widely used to describe the hysteresis characteristics of objects because of its advantages, such as fewer parameters, non-cumulative errors, and easy inversion of the model. Therefore, we also use the PI model to describe the hysteresis characteristics of piezoelectric actuators. However, to solve the problem of invalid operators in the previous PI hysteresis model with many operators and weight 0, we propose a PI hysteresis modeling method for piezoelectric actuators based on threshold optimization to eliminate the invalid operators with weight 0 in the model. In addition, in order to solve the problem that the static PI hysteresis model is difficult to accurately describe the hysteresis characteristics of piezoelectric actuators in dynamic conditions, we combine the few operator PI hysteresis model with the linear dynamic model of piezoelectric actuators to establish the PI hysteresis model of rate-dependent piezoelectric actuators. This model can not only describe the hysteresis characteristics of piezoelectric actuators in static conditions. The

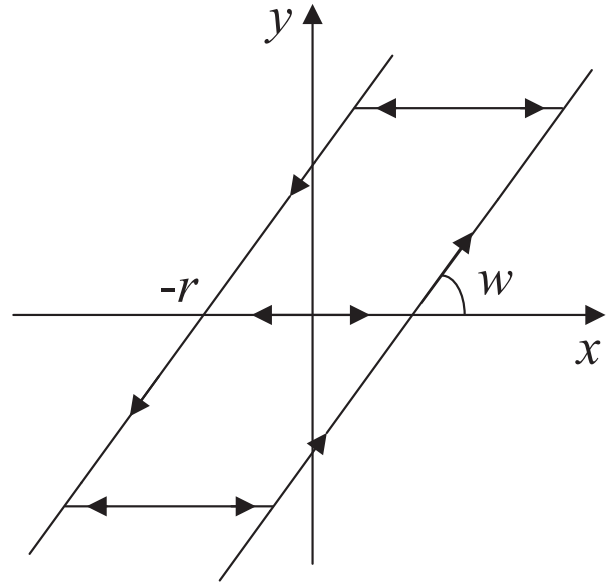


**Figure 2.** Backlash operator.

hysteresis characteristics of piezoelectric actuators can also be well described in dynamic situations.

### 2.1. Description of PI hysteresis model

PI model belongs to the operator model, which is weighted by multiple Backlash operators to fit hysteresis nonlinearity, so it can provide high accuracy, in which a single Backlash operator is shown in Figure 2.

The output expression of the Backlash operator is:

$$y(t) = H[x, y_0](t) = w \cdot \max\{x(t) - r, \min[x(t) + r, y(t - T)]\} \quad (1)$$

In the formula,  $H$  represents the Backlash operator,  $x$  and  $y$  are the input and output of the Backlash operator,  $y_0$  is the initial value of the operator output,  $w$  and  $r$  are the weight and threshold of the Backlash operator, and  $T$  is the sampling period.

Its threshold  $r$  determines each Backlash operator, and the PI hysteresis model is composed of the weighted superposition of  $n$  Backlash operators, which can be expressed as follows:

$$y(t) = \sum_{i=0}^n w_i \max\{x(t) - r_i, \min[x(t) + r_i, y_i(t - T)]\} \quad (2)$$

When the voltage from 0 to the maximum is applied to the piezoelectric ceramics, the complete hysteresis loop, that is, the initial load curve can be obtained. As shown in Figure 3, the initial load curve can be expressed as (Kuhnen and Janocha, 2001):

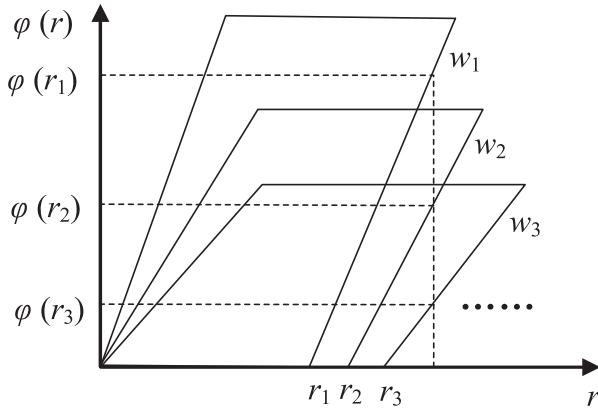


**Figure 3.** PI hysteresis model calculation diagram.

$$\varphi(r) = \sum_{j=0}^i w_j(r - r_j) ; r_i \leq r < r_{i+1} ; i = 0, 1, \dots, n \quad (3)$$

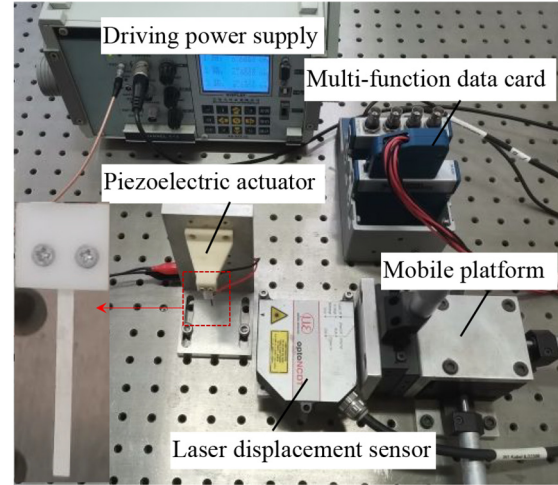
In the formula,  $r$  is the input (i.e.  $x(t)$  in formula (2)),  $\varphi(r)$  is the output (i.e.  $y(t)$  in formula (2)).

## 2.2. Static hysteresis modeling of the actuator

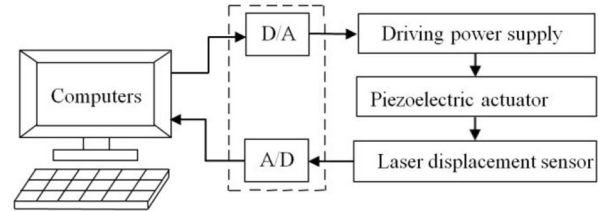
Usually, when using the PI hysteresis model to establish the hysteresis model of the object, to make the model accurate, the threshold is often divided into very small, but this makes too many operators, and most of them are invalid operators with zero weight, too many operators will reduce the response speed of the controlled object during control.

Because the slope of the initial load curve at each threshold point is expressed by the weighted sum of the hysteresis operator at each threshold point when the PI model is used to fit the measured curve of the described object, it can be seen that the closer the weighted sum of the hysteresis operator at each threshold point is to the slope of the initial load curve at this point, the higher the accuracy of the model. Accordingly, this paper proposes a threshold optimization method to reduce the number of operators, that is, under the condition that the accuracy of the model meets the requirements and the variation of the whole threshold interval is as uniform as possible, the threshold is divided according to the size of the weighted sum. In this way, the number of operators in the hysteresis model of the described object will be greatly reduced. Thus the response speed of the controlled object will be improved. In this paper, the process of dividing the threshold based on the weighted sum is as follows:

- (1) Fitting the measured initial load curve with the polynomial function;
- (2) Finding the derivative of the polynomial function at each sampling point (i.e. the slope, the slope can be regarded as the weight of the



(a)



(b)

**Figure 4.** Piezoelectric actuator experimental system: (a) experimental system photos and (b) experimental system block diagram.

hysteresis operator at the corresponding sampling point) and the sum of all the slopes;

- (3) Divide the slope sum into  $n$  equal parts, where  $n$  is the number of operators;
- (4) To obtain the threshold corresponding to the sum of the slope of each partition (the sum of the slope can be considered as the weighted sum of the hysteresis operator in each threshold interval).

Figure 4 shows an experimental system for measuring the output displacement of a piezoelectric actuator, which consists of a piezoelectric actuator, a multi-function data card (National Instruments, PCI-6221, with 16 digits and a maximum sampling frequency of 250 kS/s), a laser displacement sensor (MICRO-EPSILON, ILD2300-2, with a measuring range of 2 mm, a resolution of 30 nm, a maximum measuring signal frequency of 49.02 kHz), and an electric source driven by a piezoelectric actuator (CORE-MORROW, E01.C3, whose output voltage ripple amplitude is less than 5 mV, and its bandwidth is 1 kHz when the load is 2  $\mu$ F) and computer. The experimental process is described as follows: first, the laser displacement sensor is within the measuring range, and then the voltage generated by the Labview program is transmitted from the computer to the multi-function data card, and then

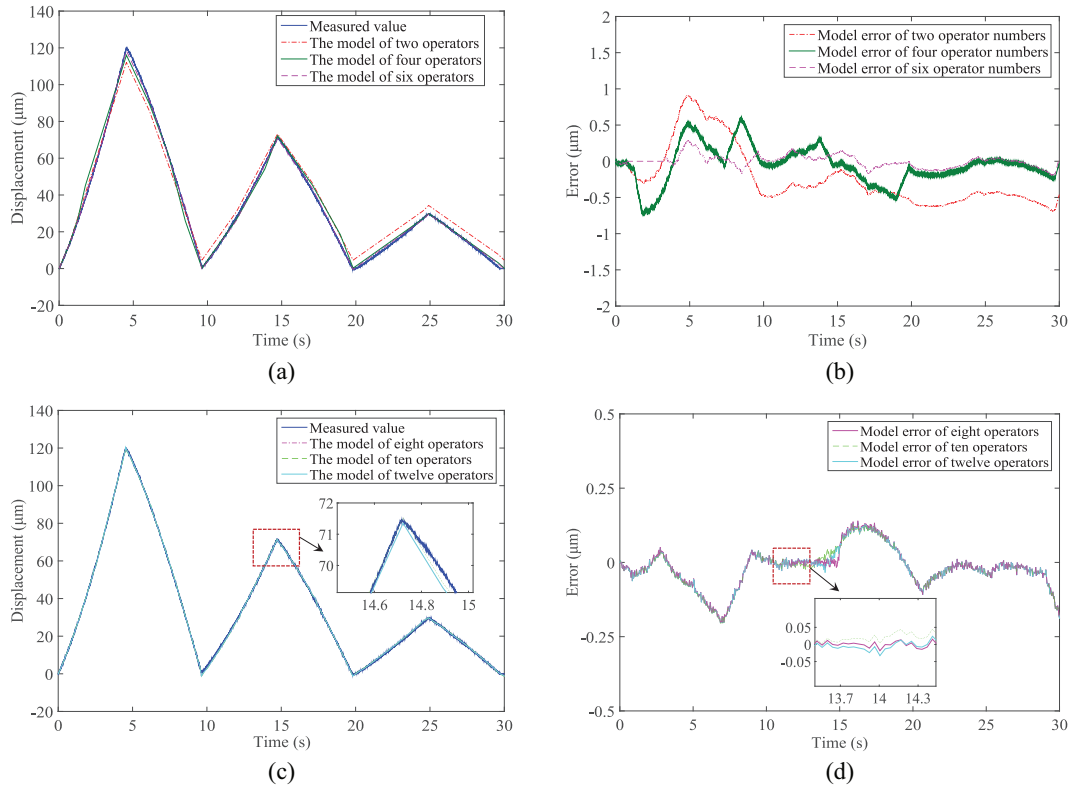


**Figure 5.** Comparison between model values and measured values of different operator numbers: (a) the model values and measured values established by 2, 4, and 6 operator numbers, (b) the error between the model value and the measured value established by 2, 4, and 6 operator numbers, (c) the model values and measured values established by 8, 10, and 12 operator numbers (d) the error between the model value and the measured value established by 8, 10, and 12 operator numbers.

the D/A converter on the data card is converted into an analog voltage-controlled piezoelectric actuator driving power supply, which outputs the corresponding driving voltage to make the actuator produce the corresponding output displacement, which is measured by the laser displacement sensor and collected into the computer by the Labview program through the network port on the computer.

Based on the experimental system shown in Figure 4, the peak values of 90, 60, and 30 V, sampling interval 1 ms, triangular wave driving voltage of 10 s per cycle are applied to the piezoelectric actuator, and the sampling frequency of the laser displacement sensor is 1 kHz. Figure 5 shows the measured curve and model curve when the operator number  $n$  is 2 to 12.

Figure 6 shows the variation of the average error with the number of operators between the measured curve and the model curve based on the proposed threshold optimization method. As shown in Figures 5 and 6, when the number of operators is  $\geq 7$ , the model error becomes stable gradually, and the decrease is not apparent. Therefore, after considering the calculation speed and model accuracy, seven Backlash operators are used to establish the hysteresis model of piezoelectric actuators. The thresholds and weights of these seven operators are shown in Table 1.

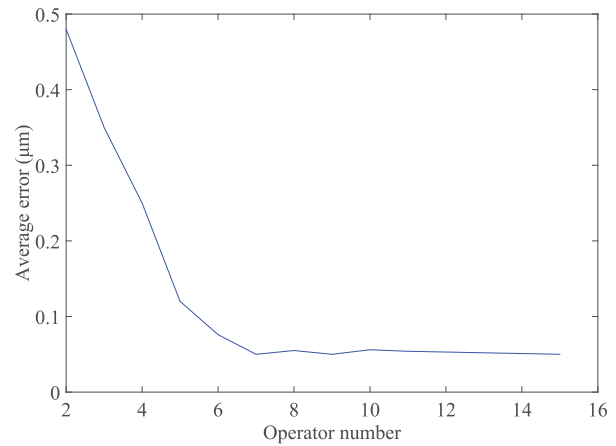


**Figure 6.** Variation of model error with the operator.

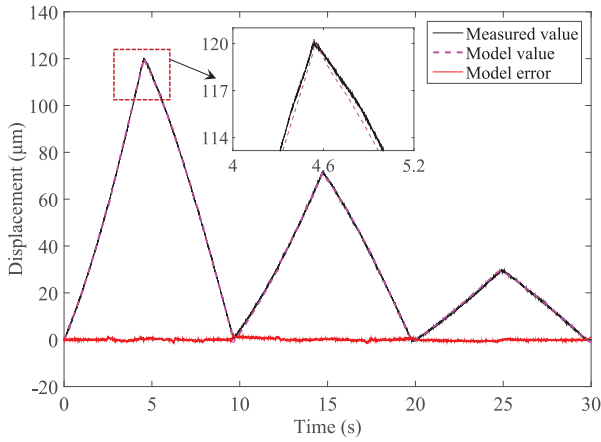
When analyzing the experimental results, the following fitness indexes are defined to evaluate the modeling accuracy of the parametric model:

$$\beta_{\text{fit}} = \left( 1 - \frac{\sum_{j=1}^N (\delta_j(t) - \hat{\delta}_j(t))^2}{\sum_{j=1}^N (\delta_j(t) - \bar{\delta})^2} \right) \times 100\% \quad (4)$$



**Table 1.** Improved parameter identification results of PI hysteresis model.

Operator number ( <i>i</i> )	Threshold value ( $r_i'$ )	Weight ( $w_i'$ )
1	0	0.15016
2	13.782	0.069841
3	24.930	0.025238
4	35.064	-0.057557
5	44.995	0.058218
6	54.926	-0.0097043
7	65.060	-0.020715

**Figure 7.** Measured and model values of hysteresis characteristics of piezoelectric actuators.

The formula  $\beta_{\text{fit}}$  indicates the degree of fit between the measured value and the model value. A large  $\beta_{\text{fit}}$  value indicates a high degree of fit, indicating that the measured figure is consistent with the model figure, and a small  $\beta_{\text{fit}}$  value indicates a low degree of fit, indicating a large gap between the measured figure and the model figure;  $N$  represents the total number of data points;

$\delta_f(t)$  represents the measured displacement data;  $\hat{\delta}_f(t)$  represents the model output date;  $\bar{\delta}$  represents the average value of the measured displacement data.

Because the lift and return in the hysteresis ring of piezoelectric material are not completely symmetrical, to improve the accuracy of the hysteresis model, the method of separately modeling the lift and return stroke is adopted for the hysteresis model of the piezoelectric actuator. Figure 7 shows the measured and model values of the hysteresis curve of the piezoelectric actuator under the triangular wave voltage with peak values of 90, 60, and 30 V, respectively. As can be seen from the figure, in the displacement range of 0–120  $\mu\text{m}$  of the piezoelectric actuator, the absolute fitting error is -1.33 to 1.98  $\mu\text{m}$ , and the fluctuation of the error curve is uniform, and the degree of fit is 96.28%. This verifies the effectiveness of the proposed threshold optimization method.

The PI hysteresis model has an analytical inverse. According to equation (3), the inverse model of the PI hysteresis model of the piezoelectric actuator can be expressed as follows:

$$\varphi'(r') = \sum_{j=0}^i w'_j(r' - r'_j); \quad r'_i \leq r' < r'_{i+1}; \quad i = 0, 1, \dots, n \quad (5)$$

In the formula,  $\varphi'(r')$  is the inverse function of  $\varphi(r)$ , and  $w'$  and  $r'$  are the weights and thresholds in the inverse model of PI hysteresis of piezoelectric actuators, respectively.

Since the PI-positive model and its inverse model of the piezoelectric actuator are inverse functions of each other, the threshold  $r'$  of the inverse model is equal to the output  $\varphi(r)$ , of the positive model, that is:

$$\begin{aligned} r' &= \varphi(r) = \sum_{j=0}^i w_j(r - r_i); \\ r'_i &\leq r' < r'_{i+1}; \quad i = 0, 1, \dots, n \end{aligned} \quad (6)$$

Similarly, because the positive model of the piezoelectric actuator PI and its inverse model is symmetrical concerning the straight line  $y = x$ , the slope at the same abscissa (i.e. the weighted sum at the threshold) is reciprocal to each other. From equation (3), the slope of the PI-positive model of the piezoelectric actuator can be expressed as follows:

$$\frac{d\varphi(r)}{dr} = \sum_{j=0}^i w_j; \quad r_i \leq r < r_{i+1}; \quad i = 0, 1, \dots, n \quad (7)$$

From equation (5), the slope of the PI inverse model of the piezoelectric actuator can be expressed as follows:

$$\frac{d\varphi'(r')}{dr'} = \sum_{j=0}^i w'_j; \quad r'_i \leq r' < r'_{i+1}; \quad i = 0, 1, \dots, n \quad (8)$$

Since formulas (7) and (8) are reciprocal to each other, it can be obtained:

$$\sum_{j=0}^i w_j = \frac{1}{\sum_{j=0}^i w'_j}; \quad i = 0, 1, \dots, n \quad (9)$$

When  $i = 0$ , there are:

$$w_0' = \frac{1}{w_0} \quad (10)$$

When  $i > 0$ , formula (8) can obtain:

**Table 2.** Average error and maximum error of output displacement of the piezoelectric actuator relative to target displacement.

Compensation method	Average error/maximum error		
	0.1 Hz (%)	10 Hz (%)	20 Hz (%)
Rate-dependent PI hysteresis compensation	2.42/3.60	2.65/3.88	2.93/4.07
PI hysteresis compensation	2.45/3.62	4.12/7.60	5.32/9.5
No hysteresis compensation	8.69/16.33	9.02/17.39	10.36/16.07

$$w_i' = -\frac{w_i}{\sum_{j=0}^i w_j \sum_{j=0}^{i-1} w_j} ; i = 0, 1, \dots, n \quad (11)$$

Formula (6) is the solution method of threshold in the PI inverse model of the piezoelectric actuator, and formulas (10) and (11) are weight solution methods. After determining  $w'$  and  $r'$ , the inverse model of PI hysteresis of the piezoelectric actuator can be determined.

### 2.3. Dynamic hysteresis modeling and compensation simulation of the actuator

The PI hysteresis model is a static model, which does not change with the change of frequency and is rate-independent. For the signal with a slightly higher frequency, the prediction effect of the model becomes worse, and with the increase of the signal frequency, the error of the rate-independent PI static model tends to increase. For this reason, we propose a rate-dependent PI hysteresis model. That is, the hysteresis characteristics of piezoelectric actuators are described by a model composed of a static hysteresis model and a dynamic linear model in series. Among them, the static hysteresis model is the few operator hysteresis models established above, and the dynamic linear model is established by the autoregressive ergodic (ARX) method. The output voltage data  $u(t)$  of the PI inverse model is taken as the input of the ARX model, and the output displacement data  $\delta(t)$  of the piezoelectric actuator is taken as the output of the ARX model. Using the MATLAB/System Identification toolbox, the ARX model is used to identify the parameters of the rational transfer function. By inverting the transfer function, the feedforward voltage used to compensate for the hysteresis of the piezoelectric actuator can be obtained.

In order to verify the effectiveness of the dynamic model, a sinusoidal input voltage with an amplitude of 30 V, a sampling interval of 1 ms, and a frequency of 0.1, 10, and 20 Hz is applied to the piezoelectric actuator. Figure 8 below shows the target displacement at different frequencies, the displacement before, and after hysteresis compensation. Table 2 below shows the relative average error and relative maximum error of the output displacement of the piezoelectric actuator relative to the target displacement before and after

compensation at different frequencies. According to Figure 8 and Table 2, both no rate-dependent and rate-dependent hysteresis compensation can reduce the hysteresis error of the piezoelectric actuator compared with the case without hysteresis compensation. Rate-dependent hysteresis compensation with the increase of frequency, the hysteresis error of piezoelectric actuator increases only slightly with the increase of frequency, but when there is no rate-dependent hysteresis compensation, with the increase of frequency, the hysteresis error of piezoelectric actuator after compensation is larger than that of the piezoelectric actuator at the same frequency. This shows that the rate-dependent hysteresis model established in this paper is effective.

According to the hysteresis feedforward model of the piezoelectric actuator obtained above, the hysteresis compensation of the piezoelectric actuator is simulated in MATLAB/Simulink, and the simulation result of hysteresis compensation is shown in Figure 9. It can be seen from the diagram that before compensation, three groups of hysteresis curves are obtained under three different voltages of 90, 60, and 30 V, which are highly nonlinear. After hysteresis compensation, the hysteresis phenomenon is eliminated.

## 3. Creep compensation

In micro-manipulation such as micro-parts assembly and cell operation, piezoelectric actuators often take tens of seconds or even thousands of seconds, and a long operation time will make the piezoelectric actuators creep. If the creep characteristics are not compensated, it will have a great impact on the accuracy of micromanipulation. Therefore, this section will introduce the method of creep compensation for piezoelectric actuators based on eliminating the hysteresis of piezoelectric actuators.

### 3.1. Creep modeling

As shown in Figure 10, under the action of constant voltage for a long time, the output displacement of the piezoelectric actuator will produce the corresponding monotone increasing curve creep, which can be described by logarithmic curve or parabola. Therefore, in order to obtain a constant target displacement of the

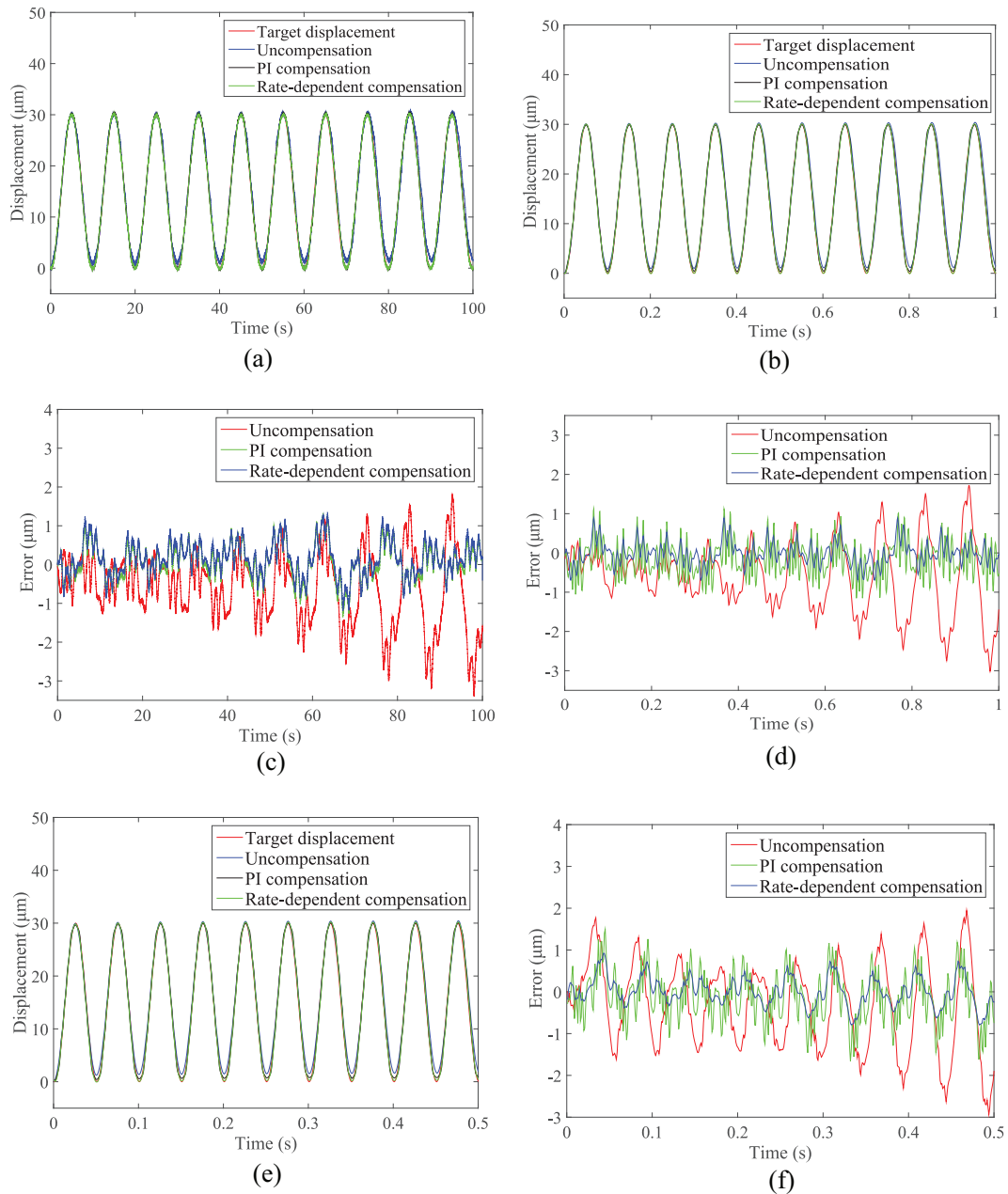


**Figure 8.** Displacement curves and errors of sinusoidal waves with different frequency inputs before and after compensation: (a) displacement curves before and after compensation under 0.1 Hz sine wave signal input, (b) relative target displacement error before and after compensation under 0.1 Hz sine wave signal input, (c) displacement curves before and after compensation under 10 Hz sine wave signal input, (d) relative target displacement error before and after compensation under 10 Hz sine wave signal input, (e) displacement curves before and after compensation under 20 Hz sine wave signal input, and (f) relative target displacement error before and after compensation under 20 Hz sine wave signal input.

piezoelectric actuator for a long time, a monotone decreasing logarithmic or parabolic driving voltage can be applied to the piezoelectric actuator.

Based on the experimental system shown in Figure 4, a step voltage with an amplitude of 30 V, a duration of 1200s, and a sampling interval of 1 ms is applied to the piezoelectric actuator, and the sampling frequency of the laser displacement sensor is 1 kHz. The results shown in Figure 11 are obtained. Within the 1200 s,

the creep displacement of the piezoelectric actuator is about 5.5  $\mu\text{m}$ . From Figure 11, we can see that the creep characteristics of piezoelectric actuators are in the shape of a logarithmic curve, so the logarithmic model can be used to describe the creep characteristics of piezoelectric actuators. Without considering the fluctuation of external stress and the change of ambient temperature, the logarithmic model to describe piezoelectric creep is given as follows:



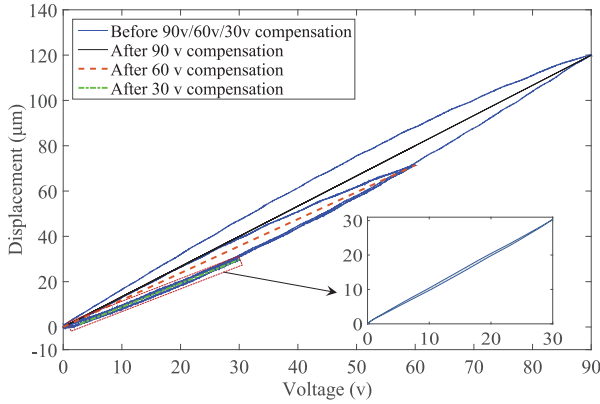


**Figure 9.** Simulation results of hysteresis compensation for piezoelectric actuators.

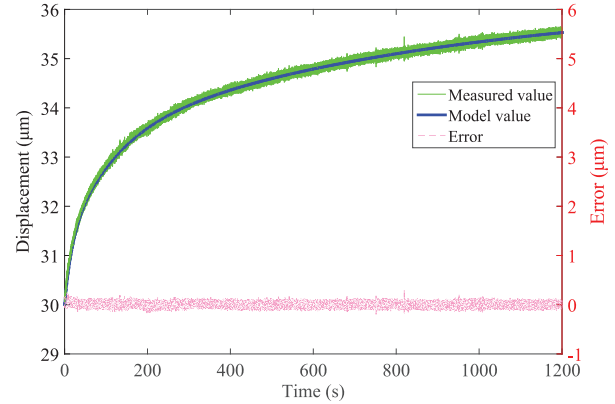


**Figure 12.** Measured and model values of displacement creep of piezoelectric actuators.

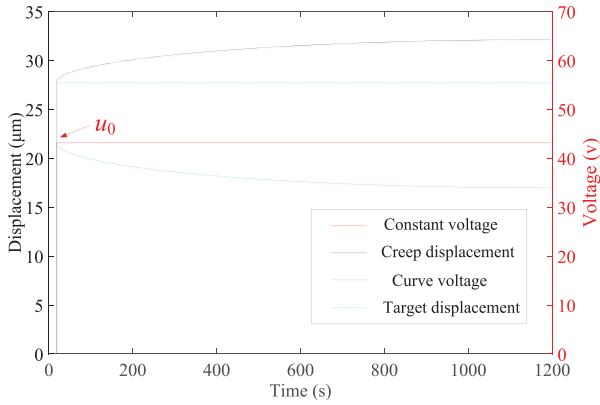


**Figure 10.** Displacement creep of the piezoelectric actuator and driving voltage schematic diagram of constant output displacement.

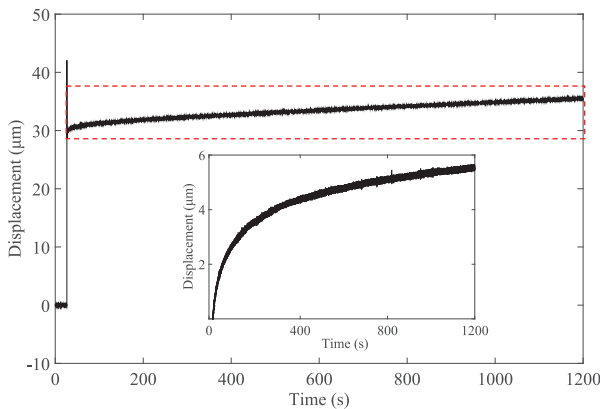


**Figure 11.** Measured displacement creep of the piezoelectric actuator.

$$\delta_c(t) = \delta_{c0} \left[ 1 + \lambda \log_{10} \left( \frac{t}{t_0} \right) \right] \quad (12)$$

In the formula,  $\delta_c(t)$  is the total output displacement of the piezoelectric actuator at a given input voltage;  $\delta_{c0}$  is

the displacement of the piezoelectric actuator after a given input voltage  $t_0$  time;  $\lambda$  is the creep coefficient of the piezoelectric actuator;  $t_0$  is the instantaneous step response time, usually  $t_0 = 0.05$  s,  $t_0$  is the timing zero of creep and  $t$  is the creep time. This logarithmic model is a creep model with a simple structure and easy to use.

The parameters of the creep curve are identified by the logarithmic model of equation (12). By using the least square curve fitting method, the following results are obtained:  $\delta_{c0} = 30$ ,  $\lambda = 0.0419$ . The fitting degree between the creep model and the measured value is 95.03%. The logarithmic creep model of the piezoelectric actuator can be expressed as follows:

$$\delta_c(t) = 30 \left[ 1 + 0.0419 \log_{10} \left( \frac{t}{0.05} \right) \right] \quad (13)$$

Figure 12 shows the measured and model curves of the creep of the piezoelectric actuator under the step voltage in Figure 11. It can be seen from the diagram that when the maximum creep reaches  $5.5 \mu\text{m}$ , if the noise of the displacement sensor is not taken into account, the deviation between the measured creep and the creep model is almost  $0 \mu\text{m}$ . It can be seen that the logarithmic model can well describe the creep characteristics of piezoelectric actuators.

### 3.2. Principle and simulation of creep compensation

From the previous analysis, it can be seen that the output displacement of the piezoelectric actuator will produce the corresponding monotone increasing logarithmic curve creep under the action of constant voltage for a long time. Therefore, to obtain a constant displacement of the piezoelectric actuator for a long time, it is necessary to apply a monotone decreasing logarithmic curve driving voltage to it. Thus, the reference formula (12), the monotone decreasing logarithmic curve driving voltage, can be expressed as:

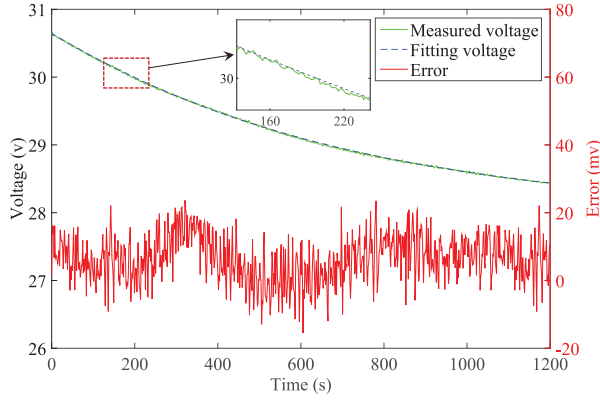


**Figure 13.** Driving voltage of piezoelectric actuators with target displacement of 30  $\mu\text{m}$ .

$$u(t) = u_0 \left[ 1 + \lambda_u \log_{10} \left( \frac{t}{t_0} \right) \right] \quad (14)$$

In the formula,  $u(t)$  is the input voltage at  $t$  time,  $u_0$  is the input voltage corresponding to  $t_0$  time at any constant displacement  $\delta_0$ , and  $\lambda_u$  is the voltage creep coefficient.

It can be seen from the formula (14) that each desired constant target displacement corresponds to a  $u_0$  and  $\lambda_u$ . It can be seen that there is a certain variation relationship between  $u_0$  and constant target displacement  $\delta$  and between  $\lambda_u$  and constant target displacement  $\delta$ . In order to obtain the above two relations, the piezoelectric actuator was shifted from 0 to 120  $\mu\text{m}$  by 6  $\mu\text{m}$  steps, that is, 6, 12, 18,..., 120  $\mu\text{m}$  gives the corresponding target displacement. A closed-loop feedback control (such as PID control) is applied to the piezoelectric actuator to obtain the driving voltage of each piezoelectric actuator under a long time (the 1200 s) constant target displacement. Figure 13 shows the driving voltage of the piezoelectric actuator during the 1200 s when the target displacement is 30  $\mu\text{m}$ . The  $u_0$  at  $t_0$  time of target displacement of 30  $\mu\text{m}$  can be obtained from this figure. According to the actual driving voltage curve, based on MATLAB/Curve Fitting Tool toolbox, and the least square method, it can fit the monotone decreasing logarithmic model curve of 30  $\mu\text{m}$  target displacement, then the  $\lambda_u$  with 30  $\mu\text{m}$  target displacement can be calculated according to the curve. Similarly, the  $u_0$  and  $\lambda_u$  under the other target displacement can be calculated, as shown in Figures 14 and 15.

Based on MATLAB/Curve Fitting Tool toolbox, and the least square method was adopted to perform curve fitting to the data point in Figure 14, the relationship between  $u_0(\delta)$  and the output displacement  $\delta$  of the piezoelectric actuator was shown as follows:

$$u_0(\delta) = \frac{344.6\delta + 280}{\delta + 346.4} \quad (15)$$

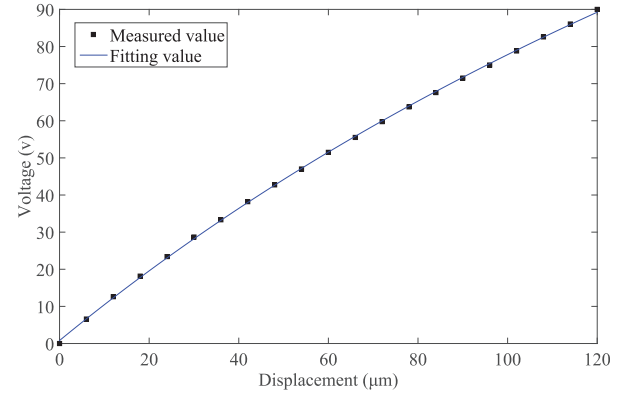


**Figure 14.** Relationship between actuating voltage and displacement of piezoelectric actuators.

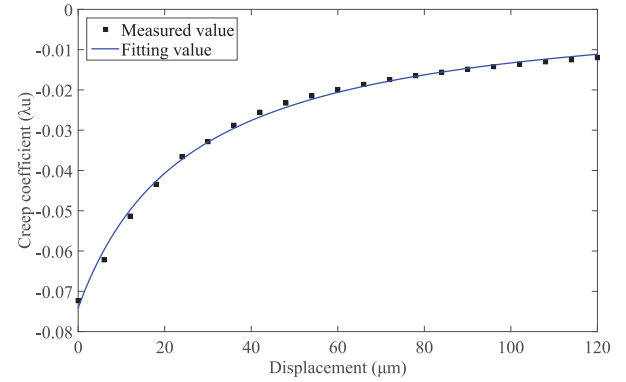


**Figure 15.** Relationship between voltage creep coefficient and displacement of piezoelectric actuators.

Where  $\delta$  is the output displacement of the piezoelectric actuator, and  $u_0(\delta)$  is the step voltage corresponding to the output displacement of the piezoelectric actuator.

Use the same method, the curve fitting of the data point in Figure 15 can be concluded that the relationship between  $\lambda_u(\delta)$  and the output displacement  $\delta$  of the piezoelectric actuator is:

$$\lambda_u(\delta) = \frac{-1.716}{\delta + 22.9} \quad (16)$$

In the formula,  $\lambda_u(\delta)$  is the voltage creep coefficient corresponding to the output displacement of the piezoelectric actuator.

Substituting equations (15) and (16) into equation (14), the driving voltage at a constant target displacement for a long time can be obtained as follows:

$$u(t) = \frac{344.6\delta + 280}{\delta + 346.4} \left[ 1 + \frac{-1.716}{\delta + 22.9} \log_{10} \left( \frac{t}{0.05} \right) \right] \quad (17)$$

According to equation (17), as long as the required output displacement of the piezoelectric actuator is given, the control voltage with the displacement

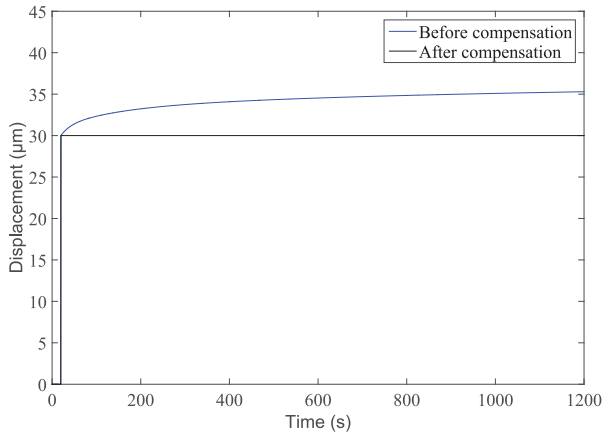


**Figure 16.** Simulation results of creep compensation for piezoelectric actuators.

remaining unchanged for a long time can be obtained, so that creep compensation can be achieved without solving the inverse.

Based on the creep compensator of the output displacement of the piezoelectric actuator given in equation (17), MATLAB/Simulink was used to simulate the creep compensation. The simulation results are shown in Figure 16. It can be seen from the figure that the creep displacement of  $5.5 \mu\text{m}$  remained before compensation, and the creep displacement was eliminated after compensation, indicating that the proposed without demand inversion creep compensation method is effective.

## 4. Dynamic compensation

As can be seen from Figure 11, the transient response process of the piezoelectric actuator produces a large overshoot due to the oscillation after the step voltage is applied. This oscillation not only affects its accuracy but also damages the clamping object or piezoelectric actuator easily. Therefore, based on eliminating hysteresis and creep of piezoelectric actuators, the oscillation modeling and suppression of piezoelectric actuators are introduced in this section.

### 4.1. Dynamic modeling

We take the oscillation phase of the experimental data in Figure 11 to identify the dynamic model of the piezoelectric actuator. In the specific identification, the measured data of the vibration stage of the piezoelectric actuator are imported into the MATLAB/System Identification toolbox. Then the ARMAX (Auto Regression and Moving Average model with eXogenous input) model is used. The second-order, third-order, and fourth-order ARMAX models are used to identify the dynamic model of the piezoelectric actuator. The degree of fit between the identified second-order, third-order, and fourth-order

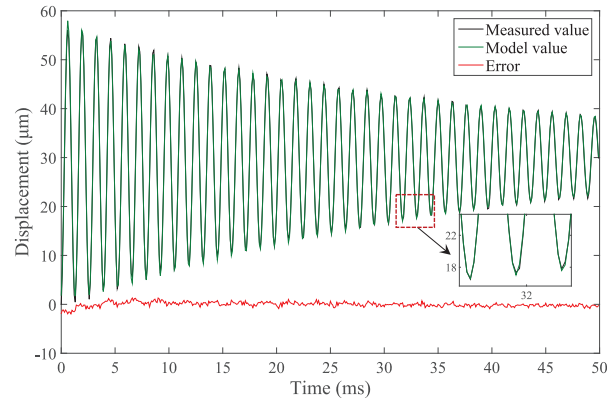


**Figure 17.** Measured and model values of vibration characteristics of piezoelectric actuators.

ARMAX models of piezoelectric actuators and the measured values are 96.12%, 96.09%, and 97.22%, respectively. Obviously, the second-order dynamic model is not only simple but also has high accuracy. Therefore, the second-order dynamic model is adopted in this paper. The second-order dynamic model of piezoelectric actuator is as follows:

$$G(s) = \frac{3.293 \times 10^6}{s^2 + 51.15s + 2.257 \times 10^7} \quad (18)$$

Figure 17 shows the comparison between the measured values of the vibration characteristics of the piezoelectric actuator and the model values after the step voltage is applied, in which the absolute fitting error of the second-order dynamic model is  $-1.95$  to  $1.31 \mu\text{m}$ , which shows that the model values are in good agreement with the measured values. Since the vibration of the piezoelectric actuator is mainly concentrated in the first 50 ms of the response, only the response of the pre-50 ms is given.

### 4.2. Principle and simulation of oscillation suppression

In the aspect of vibration suppression of piezoelectric actuators, the input shaping method (ZV) is widely used because of its simple principle and ease of implementation. However, when the damping of the system is small, its robustness becomes worse. As the damping of the piezoelectric actuator in this paper is small and the oscillation is obvious (as shown in Figure 17), the ZVD method based on the ZV method is presented in this paper. ZVD (Zero Vibration Derivative) method is to configure double zeros for the system by constraining the dynamic equation of the controlled object (i.e. derive the oscillation frequency of the controlled object and make the derivative 0) to eliminate the oscillation of the controlled object and improve the robustness.

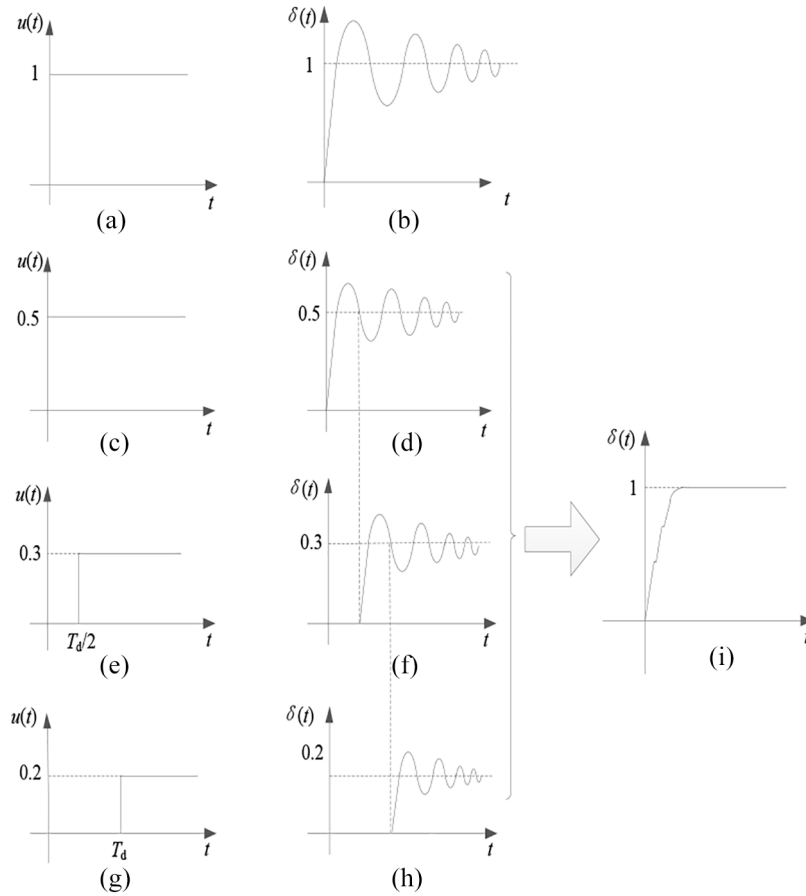


**Figure 18.** Schematic diagram of weighted pulse convolution shaping method (a) step voltage with an amplitude of 1 V, (b) oscillation output produced by the system at 1 V, (c) pulse with a weight of 0.5V, (d) the oscillation output produced by the system under the 0.5 V pulse, (e) the pulse with the weight of 0.3V at the  $T_d/2$  time, (f) the oscillation output produced by the system under the pulse of 0.3 V, (g) the pulse with the weight of 0.2 V at the  $T_d$  time, (h) the oscillation output produced by the system under the pulse of 0.2 V, (i) the output produced by the system under the combined action of the three step voltages.

The implementation of the ZVD method is described below.

According to the classical control theory, the attenuation frequency  $\omega_d$  of the system has the following relationship with the natural frequency  $\omega_n$ :

$$\omega_d = \omega_n \sqrt{1 - \xi^2} \quad (19)$$

Therefore, the attenuation period  $T_d$  can be expressed as:

$$T_d = \frac{2\pi}{\omega_n \sqrt{1 - \xi^2}} \quad (20)$$

As shown in Figure 18, if a step voltage with an amplitude of 1 is applied to the controlled object (as shown in the (a) diagram), if the system oscillation is not suppressed, the system output will oscillate (as shown in the (b) diagram); When the weighted pulse convolution oscillation shaping method (take three shaping pulses as an example) is used to restrain the

system oscillation, the original input voltage and three shaping pulses (their weights are 0.5, respectively, 0.3 and 0.2, respectively, and the weighted sum is 1) are convoluted. The result is that the amplitude of the original input voltage is 0.5, 0.3, 0.2, respectively. The time of step occurrence is 0,  $T_d/2$ , and  $T_d$  (shown by (c), (e), and (g), respectively). Under the joint action of these three-step voltages, the output produced by the system is the sum (as shown in the (i) diagram) of the output produced by the respective action of the three-step voltages (as shown in the figure of (d), (f), and (h)).

The oscillation model of the system is generally a second-order system, and the transfer function of the second-order system is as follows:

$$G(s) = \frac{K\omega_n^2}{s^2 + 2\xi\omega_n s + \omega_n^2}; 0 < \xi < 1 \quad (21)$$

When the input signal is a pulse function with amplitude  $A$ , the inverse Laplace transform of equation (21) is the impulse response  $c(t)$  of the second-order system.

$$c(t) = KA \frac{\omega_n}{\sqrt{1-\xi^2}} e^{-\xi\omega_n t} \sin \omega_d t \quad (22)$$

If the pulse sequence with the amplitude of  $A_i$  is applied at  $t_i$  time, the impulse response of the system can be expressed as follows:

$$c_i(t) = KA_i \frac{\omega_n}{\sqrt{1-\xi^2}} e^{-\xi\omega_n(t-t_i)} \sin[\omega_d(t-t_i)] \quad (23)$$

When the system is in  $t_1, t_2, \dots, t_n$  time, the applied amplitude is  $A_1, A_2, \dots, A_n$ . When the algebraic sum of the response generated by these pulse sequences is 0, the system's oscillation is eliminated. That is, the following formula is satisfied:

$$\sum_{i=1}^n c_i(t) = 0 \quad (24)$$

After the convolution operation of the input signal and the pulse signal, from the result, the original input signal is moved to the defining point of the pulse signal. Therefore, in order not to change the output gain, the algebraic sum of the amplitudes of all pulses in the pulse sequence should be 1, that is:

$$\sum_{i=1}^n A_i = 1 \quad (25)$$

It is known that the time when each pulse is applied is  $t_i$ :  $t_1 = 0, t_2 = T_d/2, \dots, t_n = (n-1)T_d/2$ . Substituting it into equation (24), there are:

$$\sum_{i=1}^n KA_i \frac{\omega_n}{\sqrt{1-\xi^2}} e^{-\xi\omega_n t} e^{\frac{n\pi\xi}{\sqrt{1-\xi^2}}} \sin(\omega_d t - n\pi) = 0 \quad (26)$$

After using the input shaper  $C(s) = \sum_{i=1}^n A_i e^{-t_i s}$ , the residual oscillation percentage of the system is a function of the natural frequency and damping coefficient of the system:

$$\begin{cases} V(\omega, \xi) = e^{-\xi\omega t_n} \sqrt{D^2 + F^2} \\ D = \sum_{i=1}^n KA_i e^{\xi\omega t_i} \sin(\omega_d t_i) \\ F = \sum_{i=1}^n KA_i e^{\xi\omega t_i} \cos(\omega_d t_i) \end{cases} \quad (27)$$

In order to improve the robustness of the system, it is necessary to satisfy not only the zero oscillation condition, that is  $V(\omega, \xi)$ , but also the equation with constraints. The derivative of this equation to  $V(\omega, \xi)$  the equation is zero, that is  $\frac{dV(\omega, \xi)}{d\omega} = 0$ . This method is called the zero oscillation derivative method, abbreviated as ZVD. This method can not only eliminate the vibration modes of the object but also restrain the influence caused by the change of parameters. The simultaneous constraint equations are as follows:

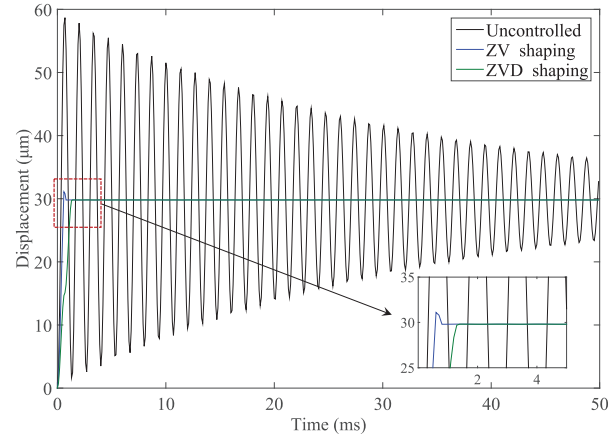


**Figure 19.** Simulation results of oscillation suppression of piezoelectric actuators.

$$\begin{cases} V(\omega, \xi) = 0 \\ \frac{dV(\omega, \xi)}{d\omega} = 0 \\ \sum_{i=1}^n A_i = 1 \\ A_i > 0 \end{cases} \quad (28)$$

Substituting the overshoot  $M = e^{\frac{-\pi\xi}{\sqrt{1-\xi^2}}}$ , according to the parity of the value of  $n$ , to satisfy equation (28), only need to satisfy:

$$\begin{cases} \sum_{i=1}^{\frac{n}{2}} \left( \frac{A_{2i-1}}{M^{2i-1}} - \frac{A_{2i}}{M^{2i}} \right) = 0, n = 2, 4, 6, \dots \\ \sum_{i=1}^{\frac{n+1}{2}} \frac{A_{2i-1}}{M^{2i-1}} - \sum_{i=1}^{\frac{n-1}{2}} \frac{A_{2i}}{M^{2i}} = 0, n = 3, 5, 7, \dots \end{cases} \quad (29)$$

The result of the complete square expansion just satisfies the above formula and then combines the formula (29). After weighting, the amplitude of each pulse of the pulse sequence is:

$$\begin{cases} A_1 = \frac{a_1}{(1+M)^{n-1}} \\ A_2 = \frac{a_2}{(1+M)^{n-1}} \\ \vdots \\ A_n = \frac{a_n}{(1+M)^{n-1}} \end{cases} \quad (30)$$

Where  $a_1, a_2, \dots, a_n$  represents the value of the expanded polynomial  $(1+M)^{n-1}$ , respectively. That is,  $a_1 = 1, a_n = M^{n-1}$ .

According to the applied time of the pulse sequence and the amplitude of the response obtained above, the simulation is carried out in Simulink, and the simulation results are shown in Figure 19. It can be seen from the figure that when the system does not add a shaper, it oscillates violently under the action of step voltage. After the ZV input shaping control, the time for the system to reach the steady-state is fast, but there is still a

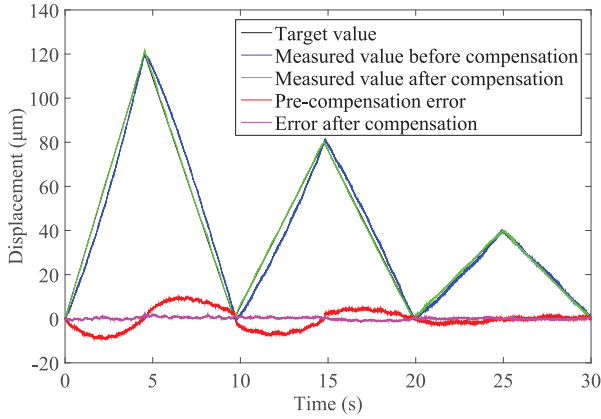


**Figure 20.** Experimental results of hysteresis compensation for piezoelectric actuators.

little overshoot, and oscillation is not allowed in subtle operations, which is not the effect we want. The ZVD input shaping control suppresses the system oscillation well, and the effect of ZVD input shaping is better than that of ZV input shaping, so it can be proved that the robustness of the ZVD input shaping method is better than that of the ZV input shaping method.

## 5. Experimental verification

### 5.1. Hysteresis compensation results

To verify the effectiveness of hysteresis compensation, based on the experimental system shown in Figure 4, the hysteresis error compensation experiment of piezoelectric actuator is carried out. The voltage applied to the piezoelectric actuator is the same as that applied in Figure 5. The experimental results of hysteresis compensation are shown in Figure 20. It can be seen from the figure that after hysteresis compensation, compared with the target value, the output displacement error of the piezoelectric actuator is reduced from  $-9.07$  to  $9.46 \mu\text{m}$  to  $-1.22$  to  $1.78 \mu\text{m}$ . The experimental results further prove the effectiveness of the improved PI model in hysteresis compensation.

### 5.2. Results of creep compensation

Based on the experimental system shown in Figure 4, the experiment of creep compensation for the piezoelectric actuator is carried out. The voltage applied to the piezoelectric actuator is the same as that applied in Figure 11, and the experimental results of creep compensation are shown in Figure 21. It can be seen from the figure that after creep compensation, the displacement creep of the piezoelectric actuator is reduced from  $5.5$  to  $0.3 \mu\text{m}$  within the  $1200$  s without considering sensor noise. This further verifies that the proposed creep controller without demand inversion has good performance in restraining the creep of piezoelectric actuators.

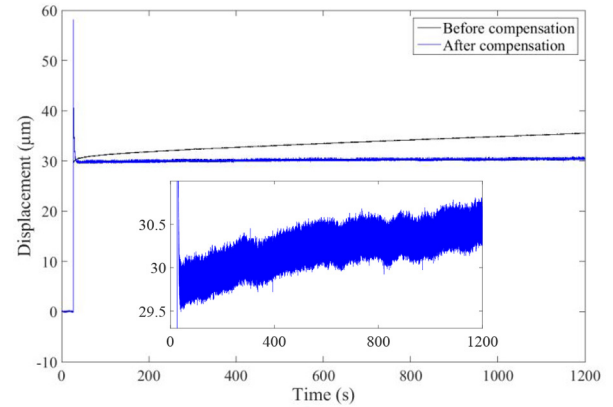


**Figure 21.** Experimental results of creep compensation for piezoelectric actuators.

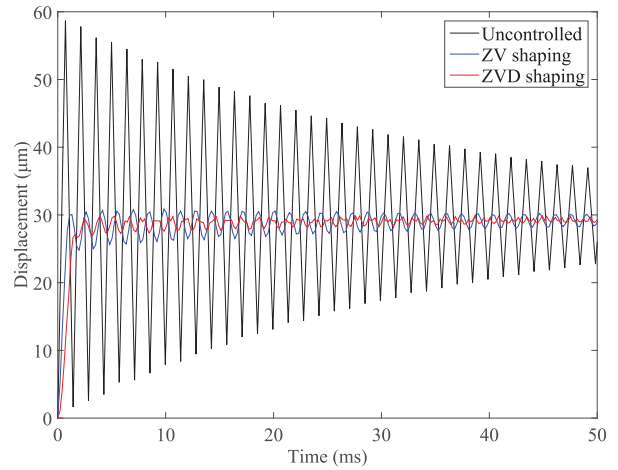


**Figure 22.** Results of concussion suppression experiment.

### 5.3. Oscillation suppression results

Based on the experimental system shown in Figure 4, the experiment of oscillation suppression of the piezoelectric actuator is carried out. The voltage applied to the piezoelectric actuator is the same as that applied in Figure 11, and the experimental results of oscillation suppression are shown in Figure 22. It can be seen from the figure that after ZV shaping control, the displacement overshoot of the piezoelectric actuator is reduced to  $2.9\%$  of that before shaping control, while after ZVD shaping control, the displacement overshoot is reduced to  $0.6\%$  of that before shaping control. This further shows that the ZVD input shaping method is more robust than the ZV input shaping method in suppressing the displacement oscillation of piezoelectric actuators.

### 5.4. Comparison and analysis

The experimental results of precision open-loop control are compared with those of classical PID closed-loop control (Tian et al., 2020) and compound control (Cai



**Table 3.** Comparison of experimental data between precision open-loop control, closed-loop control, and compound control.

Experimental data	Range of motion ( $\mu\text{m}$ )	Overshoot ( $\mu\text{m}/\%$ )	Response time (ms)	Adjusting time (ms)	Steady-state error ( $\mu\text{m}/\%$ )
Precision open-loop control	30	1.1/3.6	1.48	50	0.72/2.4
PID control	10	0.7/7	15	56	0.17/1.7
Compound control	6.9	1.3/18.8	1.5	21	0.175/2.54

et al., 2016), respectively (different control methods are for the piezoelectric actuators of their respective control objects). As shown in Table 3, the precision open-loop control is close to compound control and PID closed-loop control in terms of steady-state error and adjusting time, respectively. In micro-assembly and micro-operating systems, the precision of precision open-loop control has met the needs, and the overshoot of precision open-loop control is only 3.6%. The response speed is faster, which is 1.48 ms. It can be seen that the precision open-loop control has achieved the comprehensive performance of closed-loop control and compound control. It is of great significance to reduce the cost of micro-assembly and micro-operating systems and to ensure that the system still has high operation accuracy when the space is limited.

## 6. Conclusions

This paper presents an open-loop control method for hysteresis, creep compensation, and oscillation suppression of piezoelectric actuators. The control scheme consists of four steps: first, based on the PI model and the proposed threshold partition method, the hysteresis model of the piezoelectric actuator with rate-dependent and few operators is established. The PI hysteresis model with few operators can improve the response speed of the controlled object without affecting the accuracy of the model, and then the inverse model is used to compensate for the hysteresis error of the piezoelectric actuator. In the second step, the creep model of the logarithmic piezoelectric actuator with simple expression and few parameters is established, and a creep controller without demand inversion is designed. In the third step, aiming at the oscillation of the system, a ZVD input shaping method with good robustness is presented. By convolution between the input and a group of shaping pulses, the result is used as a new input, which basically eliminates the displacement oscillation of the piezoelectric actuator. Finally, the hysteresis, creep compensator, and oscillation suppression controller are connected in series with the piezoelectric actuator step by step, and the precise open-loop control scheme of hysteresis and creep compensation, and oscillation suppression of the piezoelectric actuator is realized.

The experimental results verify the effectiveness of the open-loop control method. After hysteresis compensation, the voltage-displacement error of the piezoelectric actuator is reduced from  $-9.07$  to  $9.46 \mu\text{m}$  to  $-1.22$  to  $1.78 \mu\text{m}$  when the maximum displacement is  $120 \mu\text{m}$ . After creep compensation, the creep of actuator displacement is reduced from  $5.5$  to  $0.3 \mu\text{m}$  within the  $1200$  s. After oscillation control, the displacement overshoot of the piezoelectric actuator is reduced to  $0.6\%$  of that before control. These results show that the precision open-loop control of the piezoelectric actuator can improve the performance of the system.


## Declaration of conflicting interests

The author(s) declared no potential conflicts of interest with respect to the research, authorship, and/or publication of this article.

## Funding

The author(s) disclosed receipt of the following financial support for the research, authorship, and/or publication of this article: This research was funded by the National Natural Science Foundation of China (No.52075273).

## ORCID iD

Yuguo Cui  <https://orcid.org/0000-0001-6636-4470>

## References

- Al Janaideh M, Rakotondrabe M, Al-Darabsah I, et al. (2018) Internal model-based feedback control design for inversion-free feedforward rate-dependent hysteresis compensation of piezoelectric cantilever actuator. *Control Engineering Practice* 72: 29–41.
- Cai K, Tian Y, Wang F, et al. (2016) Development of a piezo-driven 3-DOF stage with T-shape flexible hinge mechanism. *Robotics and Computer-Integrated Manufacturing* 37: 125–138.
- Changhai R and Lining S (2005) Hysteresis and creep compensation for piezoelectric actuator in open-loop operation. *Sensors and Actuators A: Physical* 122(1): 124–130.
- Chen X, Su CY, Li Z, et al. (2016) Design of implementable adaptive control for micro/nano positioning system driven by piezoelectric actuator. *IEEE Transactions on Industrial Electronics* 63(10): 6471–6481.
- Gan J, Zhang X, Li H, et al. (2017) Full closed-loop controls of micro/nano positioning system with nonlinear hysteresis using micro-vision system. *Sensors and Actuators A: Physical* 257: 125–133.

- Gao S, Guo R, Shao M, et al. (2020) A touch orientation classification-based force–voltage responsivity stabilization method for piezoelectric force sensing in interactive displays. *IEEE Sensors Journal* 20(14): 8147–8154.
- Garcés-Schröder M, Leester-Schädel M, Schulz M, et al. (2015) Micro-Gripper: A new concept for a monolithic single-cell manipulation device. *Sensors and Actuators A: Physical* 236: 130–139.
- Gu GY, Zhu LM, Su CY, et al. (2016) Modeling and control of piezo-actuated nanopositioning stages: A survey. *IEEE Transactions on Automation Science and Engineering* 13(1): 313–332.
- Habibullah, Pota, H. R., Petersen, I. R., & Rana, M. S. (2013). Creep, hysteresis, and cross-coupling reduction in the high-precision positioning of the piezoelectric scanner stage of an atomic force microscope. *IEEE Transactions on Nanotechnology*, 12(6), 1125–1134. <https://doi.org/10.1109/TNANO.2013.2280793>
- Heriban D, Gauthier M and Gendreau D (2008) Modular robotic platform for silicon micromechanical assembly. In 6th International Workshop on Microfactories, IWMF'08. (No. sur CD ROM, pp. 440–445).
- Jiaqiang E, Qian C, Zhu H, et al. (2017) Parameter-identification investigations on the hysteretic Preisach model improved by the fuzzy least square support vector machine based on adaptive variable chaos immune algorithm. *Journal of Low Frequency Noise Vibration and Active Control* 36(3): 227–242.
- Kim B, Washington GN and Yoon HS (2012) Hysteresis-reduced dynamic displacement control of piezoceramic stack actuators using model predictive sliding mode control. *Smart Materials and Structures* 21(5):055018–31. DOI: 10.1088/0964-1726/21/5/055018.
- Kim K, Liu X, Zhang Y, et al. (2008) Nanonewton force-controlled manipulation of biological cells using a monolithic MEMS microgripper with two-axis force feedback. *Journal of Micromechanics and Microengineering* 18(5):055013–21. DOI: 10.1088/0960-1317/18/5/055013
- Krejčí P and Monteiro G (2019) Inverse parameter-dependent Preisach operator in thermo-piezoelectricity modeling. *Discrete and Continuous Dynamical Systems: Series B* 24(7): 3051–3066.
- Kuhnen K and Janocha H (2001) Inverse feedforward controller for complex hysteretic nonlinearities in smart-material systems. *Control and Intelligent Systems* 29: 1–27.
- Lee C and Salapaka SM (2009) Robust broadband nanopositioning: Fundamental trade-offs, analysis, and design in a two-degree-of-freedom control framework. *Nanotechnology* 20(3):035501–17. DOI: 10.1088/0957-4484/20/3/035501.
- Lee SH, Royston TJ and Friedman G (2000) Modeling and compensation of hysteresis in piezoceramic transducers for vibration control. *Journal of Intelligent Material Systems and Structures* 11(10): 781–790.
- Li J, Huang H and Morita T (2019) Stepping piezoelectric actuators with large working stroke for nano-positioning systems: A review. *Sensors and Actuators A: Physical* 292: 39–51.
- Li JW, Chen XB and Zhang WJ (2010) A new approach to modeling system dynamics-in the case of a piezoelectric actuator with a host system. *IEEE/ASME Transactions on Mechatronics* 15(3): 371–380.
- Li Z, Zhang X, Su CY, et al. (2015) Nonlinear control of systems preceded by Preisach hysteresis description: A prescribed adaptive control approach. *IEEE Transactions on Control Systems Technology* 24(2): 451–460.
- Liaw HC and Shirinzadeh B (2008) Robust generalized impedance control of piezo-actuated flexure-based four-bar mechanisms for micro/nanomanipulation. *Sensors and Actuators A: Physical* 148(2): 443–453.
- Lin CJ and Lin PT (2012) Tracking control of a biaxial piezo-actuated positioning stage using generalized Duhem model. *Computers & Mathematics with Applications* 64(5): 766–787.
- Lin J, Lu M and Zhou X (2016) Development of a non-resonant 3D elliptical vibration cutting apparatus for diamond turning. *Experimental Techniques* 40: 173–183.
- Liu Y, Shan J and Qi N (2013) Creep modeling and identification for piezoelectric actuators based on fractional-order system. *Mechatronics* 23(7): 840–847.
- Lu H, Shang W, Xie H, et al. (2018) Ultrahigh-precision rotational positioning under a microscope: Nanorobotic system, modeling, control, and applications. *IEEE Transactions on Robotics* 34(2): 497–507.
- Qian C, Ouyang Q, Song Y, et al. (2020) Hysteresis modeling of piezoelectric actuators with the frequency-dependent behavior using a hybrid model. *Proceedings of the Institution of Mechanical Engineers, Part C: Journal of Mechanical Engineering Science* 234(9): 1848–1858.
- Qin Y, Zhao X and Zhou L (2017) Modeling and identification of the rate-dependent hysteresis of piezoelectric actuator using a modified Prandtl-Ishlinskii model. *Micromachines* 8(4): 114.
- Sabarianand DV, Karthikeyan P and Muthuramalingam T (2020) A review on control strategies for compensation of hysteresis and creep on piezoelectric actuators based micro systems. *Mechanical Systems and Signal Processing* 140: 106634.
- Schitter G, Allgöwer F and Stemmer A (2004) A new control strategy for high-speed atomic force microscopy. *Nanotechnology* 15(1): 108–114.
- Schröter F and Schmidt E (2018) Micromanipulation of spherical particles during condensation and evaporation of water in an environmental scanning electron microscope. *Powder Technology* 330: 80–92.
- Son NN, Van Kien C and Anh HPH (2020) Parameters identification of Bouc–Wen hysteresis model for piezoelectric actuators using hybrid adaptive differential evolution and Jaya algorithm. *Engineering Applications of Artificial Intelligence* 87: 103317.
- Tanaka Y (2014) A peristaltic pump integrated on a 100% glass microchip using computer controlled piezoelectric actuators. *Micromachines* 5(2): 289–299.
- Tan X and Baras JS (2004) Adaptive inverse control of hysteresis in smart materials. *IFAC Proceedings Volumes* 37(13): 1473–1478.
- Tian Y, Ma Y, Wang F, et al. (2020) A novel XYZ micro/nano positioner with an amplifier based on L-shape levers and half-bridge structure. *Sensors and Actuators A: Physical* 302: 111777.
- Wang G and Chen G (2017) Identification of piezoelectric hysteresis by a novel Duhem model based neural network. *Sensors and Actuators A: Physical* 264: 282–288.

- Xu Q and Li Y (2010) Dahl model-based hysteresis compensation and precise positioning control of an XY parallel micromanipulator with piezoelectric actuation. *Journal of Dynamic Systems Measurement and Control* 132(4): 1–12.
- Xu Q and Member S (2016) Digital integral terminal sliding mode predictive control of piezoelectric-driven motion system. *Control of Piezoelectric-Driven Motion System* 63(6): 3976–3984.
- Zainal M, Sahlan S and Ali M (2015) Micromachined shape-memory-alloy microactuators and their application in biomedical devices. *Micromachines* 6: 879–901.